Frontiers in Bioscience Landmark

Front. Biosci. (Landmark Ed) **2026**; 31(10): 54145
https://doi.org/10.31083/FBL54145

Original Research

Mechanisms of Diabetic Myocardial Injury Through the Lipid Droplet–Mitochondrial Pathway

Liang Wang[1,2], Jing-ya Li[1], Chuan-zhi Zhao[1], Hui-min Ding[1], Zi-qing Hu[1], Peng Zhou[1,2,*], Hui Shi[2,3,*]

[1]School of Integrated Traditional Chinese and Western Medicine, Anhui University of Chinese Medicine, 230012 Hefei, Anhui, China
[2]Anhui Provincial Key Laboratory of Chinese Medicinal Formula, 230038 Hefei, Anhui, China
[3]Nursing School, Anhui University of Chinese Medicine, 230012 Hefei, Anhui, China
*Correspondence: zhoupeng@ahtcm.edu.cn (Peng Zhou); ymf149@126.com (Hui Shi)
Academic Editor: Rajesh Katare
Submitted: 22 May 2026 Revised: 30 July 2026 Accepted: 3 August 2026 Published: 21 October 2026

Abstract

Background: Dysregulated lipid metabolism in diabetes contributes to myocardial lipotoxicity, mitochondrial dysfunction, and inflammatory cell death. This study investigated the mechanisms by which abnormal lipid metabolism in diabetes induces mitochondrial oxidative stress, and whether the lipid droplet (LD)–mitochondrial pathway is involved in cardiomyocyte pyroptosis during diabetic cardiomyopathy (DCM). **Methods:** db/db and db/m mice were evaluated for blood glucose and lipid levels, myocardial histopathologic characteristics, and cardiac function. Differentially expressed genes were identified by transcriptomic analysis, followed by Gene Ontology (GO) and Kyoto Encyclopedia of Genes and Genomes (KEGG) enrichment analyses. Immunohistochemistry and TUNEL staining were performed to assess inflammatory responses and cell death, respectively. Myocardial lipid deposition, LD distribution, mitochondrial ultrastructure, and perilipin 5 (PLIN5) expression were examined. *In vitro*, H9c2 cardiomyocytes were transfected with a PLIN5 overexpression plasmid. Immunofluorescence and Real-Time Quantitative PCR (RT-qPCR) were used to assess pyroptosis-related markers, including NLR Family, Pyrin Domain Containing Protein 3 (NLRP3), caspase 1, and Gasdermin Domain Containing 1 (GSDMD). Lipid peroxidation and reactive oxygen species (ROS) levels were measured using fluorescence-based assays. Oxygen consumption rate (OCR) was assessed using a Seahorse XFe96 analyzer, and LD–mitochondrial colocalization was evaluated by laser confocal microscopy. **Results:** Compared with db/m mice, db/db mice showed significantly increased body weight and serum levels of glucose, total cholesterol (TC), triglyceride (TG), and low-density lipoprotein cholesterol (LDL-C), together with reduced high-density lipoprotein cholesterol (HDL-C) levels ($p < 0.01$). The db/db mice also exhibited aggravated pathological changes and reduced ejection fraction (EF) and fractional shortening (FS) ($p < 0.01$). Transcriptomic analysis showed significant upregulation of fatty acid-binding protein 3 (FABP3), Long-chain acyl-CoA synthetase 1 (ACSL1), Medium-chain acyl-CoA dehydrogenase (ACADM), acyl-CoA thioesterase 2 (ACOT2), and PLIN5 in myocardial tissue. db/db mice exhibited marked myocardial lipid accumulation and increased LD abundance, accompanied by mitochondrial structural abnormalities and altered LD–mitochondrial co-localization. Total PLIN5 protein and *Plin5* mRNA expression were significantly increased, whereas mitochondrial-associated PLIN5 protein expression was significantly decreased ($p < 0.01$). In palmitic acid (PA)-treated H9c2 cardiomyocytes, immunofluorescence showed a significant increase in pyroptosis-positive cells, and protein levels of NLRP3, interleukin-1 beta (IL-1β), interleukin-6 (IL-6), interleukin-18 (IL-18), and tumor necrosis factor-α (TNF-α) ($p < 0.05$ or $p < 0.01$) were significantly increased. PLIN5 overexpression significantly reduced lipid peroxidation and ROS accumulation ($p < 0.01$), decreased maximal OCR, increased LD–mitochondrial co-localization, and reduced pyroptosis ($p < 0.01$). PLIN5 overexpression also significantly decreased NLRP3, caspase-1, and GSDMD protein and mRNA levels ($p < 0.01$). **Conclusions:** PLIN5 overexpression increased LD–mitochondrial co-localization and was associated with reduced lipid peroxidation, ROS accumulation, and activation of the NLRP3/caspase-1/GSDMD pathway in PA-treated cardiomyocytes. The PLIN5-regulated LD–mitochondrial pathway may therefore represent a mechanism linking abnormal lipid metabolism to cardiomyocyte pyroptosis and a potential therapeutic target for further investigation in DCM.

Keywords: diabetic cardiomyopathy; lipid droplets; mitochondria; Perilipin 5; NLRP3

1. Introduction

Diabetes mellitus (DM) is a major chronic noncommunicable disease that poses a serious threat to human health and continues to increase in prevalence worldwide [1]. According to the International Diabetes Federation, approximately 537 million adults currently live with DM, and this number is projected to reach 784 million by 2045 [2]. DM is associated with a 2- to 3-fold increased risk of cardiovascular disease (CVD), with CVD accounting for approximately 30%–40% of deaths among patients with DM [3]. The Framingham study further demonstrated that DM increases the risk of heart failure (HF) by 2- to 5-fold [4]. Cardiovascular complications, particularly those affecting cardiac structure and function and ultimately leading to HF,

Copyright: © 2026 The Author(s). Published by IMR Press.
This is an open access article under the CC BY 4.0 license.

Publisher's Note: IMR Press stays neutral with regard to jurisdictional claims in published maps and institutional affiliations.

are major causes of mortality in patients with DM [5]. Diabetic cardiomyopathy (DCM) is a special cardiac complication of DM, with HF representing its principal clinical manifestation and outcome, characterized by damage to the structure and function of the heart, including ventricular dysfunction, myocardial hypertrophy, interstitial fibrosis, and metabolic disorders [6,7,8]. DCM is currently considered to arise from disturbances in blood glucose and lipid metabolism that alter myocardial substrate utilization and energy production, followed by mitochondrial and other organelle dysfunction, oxidative stress, immune dysregulation, and local inflammatory responses [9,10,11]. However, the underlying mechanisms of DCM remain incompletely understood.

Dyslipidemia plays an important role in the development of cardiovascular complications associated with DM. Patients with DM, particularly those with type 2 diabetes mellitus (T2DM), frequently present with abnormalities in lipid metabolism. The *Chinese Expert Consensus on Lipid Management in Diabetic Patients (2024 Edition)* indicates that patients with T2DM commonly have elevated free fatty acids (FFAs) and triglycerides (TGs), reduced high-density lipoprotein cholesterol (HDL-C), and mildly elevated or normal total cholesterol (TC) and low-density lipoprotein cholesterol (LDL-C), primarily as a result of insulin resistance or relative insulin deficiency [12]. Lipid accumulation is an important pathological feature of DCM. In T2DM, elevated circulating FFA levels increase myocardial FFA uptake and utilization. When FFA uptake exceeds the capacity for oxidative utilization, excess lipids accumulate within myocardial tissue [13]. Although this process may initially occur without obvious clinical symptoms, progressive disruption of the balance between myocardial fatty acid uptake and oxidation can lead to diastolic dysfunction, compensatory and decompensated myocardial remodeling, and ultimately HF [14,15]. Mitochondrial dysfunction is considered a key pathogenic feature of DCM. Insulin resistance or insulin deficiency suppresses myocardial glucose uptake and utilization, resulting in a shift in cardiac energy metabolism toward fatty acid oxidation [16]. Increased fatty acid transport and utilization place a higher metabolic burden on cardiomyocytes, which increasingly depend on fatty acid β-oxidation as their primary energy source. This metabolic shift reduces the efficiency of cellular energy production and is accompanied by increased oxygen consumption and excessive generation of reactive oxygen species (ROS). When ROS production exceeds the capacity of endogenous antioxidant systems, oxidative stress develops, contributing to cardiomyocyte injury and death as well as myocardial interstitial fibrosis [17].

Activation of caspase-1 promotes the cleavage of gasdermin D (GSDMD), initiating pyroptosis, a form of inflammatory programmed cell death that has been implicated in DM and its complications [18,19]. Pyroptosis is characterized by increased cell membrane permeability and the release of pro-inflammatory cytokines and may be triggered by hyperglycemia during the development of DCM [20]. GSDMD is a key effector of pyroptosis. Upon activation by inflammatory caspases, GSDMD is cleaved into an N-terminal fragment (GSDMD-N) with pore-forming activity and a C-terminal fragment (GSDMD-C) that exerts an inhibitory effect. GSDMD-N oligomerizes and forms pores in the cell membrane, facilitating the release of inflammatory mediators such as IL-1β and IL-18 and promoting the inflammatory response [21]. Abnormal lipid metabolism in DM generates bioactive lipid molecules that can act as important triggers and endogenous regulators of pyroptosis [22]. These lipid molecules may promote pyroptosis through several mechanisms, including ROS generation, endoplasmic reticulum stress (ERS), mitochondrial dysfunction, and lysosomal damage [23].

The lipid droplet–mitochondrial pathway has emerged as a potential regulatory mechanism of pyroptosis. Lipid droplets (LDs) are important intracellular sites for lipid storage and metabolism and play a key role in maintaining lipid and energy homeostasis by storing and mobilizing fatty acids and other lipids [24]. In cardiomyocytes, LDs contribute to cardiac lipid homeostasis through the synthesis, storage, and mobilization of lipids and interact with mitochondria and the endoplasmic reticulum to establish organelle contact sites. These contact sites facilitate the exchange of lipids, ions, and other molecular components through locally regulated transport mechanisms [25]. Interactions between LDs and mitochondria facilitate lipid transfer and contribute to the regulation of cellular energy homeostasis [26]. Therefore, elucidating how LD–mitochondrial contacts regulate lipid transport and mitochondrial energy metabolism may provide important insights into the physiological functions of LDs and the role of the LD–mitochondrial pathway in the pathological process of DCM.

In this study, *in vivo* and *in vitro* experiments were performed to investigate the regulatory mechanisms of the LD–mitochondrial pathway in DCM, providing new insights into the relationship between lipid metabolism, mitochondrial dysfunction, and pyroptosis in the pathogenesis of DCM.

2. Materials and Methods

2.1 Animals

Eight male db/db mice and eight male db/m mice (specific pathogen-free [SPF] grade, 13 weeks old) were obtained from Changzhou Kawensi Laboratory Animal Co., Ltd. (SCXK (Su) 2021-0013). The db/db mice were derived from the C57BLKS strain and carried a mutation in the *Lepr* gene, resulting in spontaneous obesity and hyperglycemia. All mice were fed a standard diet and housed in cages measuring 380 × 178 × 139 mm. The animal study was conducted in accordance with the ARRIVE guidelines.

2.2 Chemicals and Reagents

Eosin staining solution (G1005-2), hematoxylin staining solution (G1005-1), MASSON staining kit (G1006), WGA staining kit (GDP1020), RNA extraction solution (G3013), SYBR (G3326-05), Hoechst 33342 staining solution (G1127), TUNEL staining kit (GDP1041), Oil Red O staining kit (GP1067), IL-6 antibody (GB300007), IL-1β antibody (GB300002), and TNF-α antibody (GB300031) were purchased from Servicebio. The perilipin 5 (PLIN5) antibody (L0219) was purchased from Santa Cruz Biotechnology (USA). The GAPDH antibody (380626) was purchased from Chengdu Zenbio Biotechnology Co., LTD. The VDAC1 antibody (00118328) was purchased from Proteintech. The NLRP3 (ab263899) and GSDMD (ab219800) antibodies were purchased from Abcam. Cleaved-Caspase 1 (AF4005) was purchased from Affinity. The glucose (GLU) kit (C050-g) and the triglyceride (TG) kit (C061-A) were purchased from Changchun Huili Biotechnology Co., LTD. The TC kit (A111-1-1) and LDL-C kit (A113-1-1) were purchased from Nanjing Jiancheng Bioengineering Institute. The HDL-C kit (A0-10137) was purchased from Zhejiang Dongou Diagnostic Products Co., LTD. The lipid fluorescence staining kit (G1264) and mitochondrial red fluorescent probe (M9940) were purchased from Solarbio. Albumin Bovine V (fatty acid-free) was purchased from G-CLONE. ECL chemical substrate luminescence kit (BL520B), Reverse transcription kit (BL696A), penicillin-streptomycin solution (BL505A), fetal bovine serum (BL201A), and ROS detection kit (BL714A) were purchased from Biosharp. Mito-Tracker Red CMXRos (C1049B) was purchased from Beyotime Biotechnology. H9c2 cells (CL-0089) were purchased from Wuhan Procell Biotechnology Co., Ltd. The plasmid was constructed using the PEX-3 cloning vector (pGCMV/MCS/Neo), with XhoI and EcoRI as the cloning sites, and was provided by GenePharma. Seahorse XF Cell Mito Stress Test kit (103015-100) and Seahorse XF DMEM medium (103575-100) were obtained from Agilent. SuperKine™ Lipo3.0 high-efficiency transfection reagent (BMU111) was purchased from Abbkine.

2.3 In Vivo Experiments

2.3.1 Detection of Cardiac Mass Index

Mice were anesthetized by intraperitoneal injection of 3% pentobarbital sodium (30 mg/kg). After cervical dislocation, the heart was surgically removed under sterile conditions. The cardiac mass index was calculated as the heart weight-to-tibial length ratio (HW/TL), where HW represents heart weight (mg), and TL represents tibial length (cm):

Cardiac mass index (HW/TL) = heart weight (mg) / tibial length (cm)

2.3.2 Blood Glucose and Cholesterol Detection

Blood samples were collected from mice into anticoagulant tubes and allowed to stand at room temperature for 2 h before centrifugation at 3000 rpm for 10 min to obtain serum. Serum levels of TC, TG, LDL-C, and HDL-C were measured using the corresponding commercial assay kits according to the manufacturers' instructions.

2.3.3 Myocardial Histopathology Detection

Ventricular tissue was cut into approximately 2-mm-thick sections, fixed and embedded in paraffin, and then sectioned at a thickness of 5 μm. Hematoxylin and eosin (HE), MASSON, and WGA staining were performed to assess pathological changes and myocardial structural remodeling.

2.3.4 Evaluation of Cardiac Function

Mice were anesthetized by isoflurane inhalation, and the anterior chest region was depilated before application of ultrasound coupling gel. The probe was positioned on the left side of the sternum. M-mode echocardiography was performed in the parasternal long-axis view of the left ventricle. Left ventricular motion curves were recorded and cardiac parameters were measured under two-dimensional image guidance. After echocardiographic examination, isoflurane administration was discontinued, and the mice were allowed to recover. Ejection fraction (EF) and fractional shortening (FS) were measured to assess cardiac function.

2.3.5 Detection of Differentially Expressed Genes

Total RNA was extracted, and mRNA was enriched using oligo(dT) beads and fragmented. Random primers were added for cDNA synthesis, followed by end repair, A-tailing, and adaptor ligation. PCR amplification was then performed, and the amplified products were recovered. Circular DNA molecules were generated and amplified by rolling-circle amplification to produce DNA nanospheres. Sequencing was performed on the DNBSEQ platform. Differentially expressed genes (DEGs) were identified using a threshold of $|\log2FoldChange| > 1$ and $p < 0.05$. The identified DEGs were visualized using volcano plots and heatmaps. Gene Ontology (GO) and Kyoto Encyclopedia of Genes and Genomes (KEGG) enrichment analyses were performed to investigate the biological functions and pathways associated with the DEGs.

2.3.6 Immunohistochemical Detection of Inflammatory Proteins

Following anesthesia, mice were euthanized by cervical dislocation, and the hearts were surgically removed under sterile conditions. The heart tissues were fixed in 4% paraformaldehyde for 24 h, dehydrated, embedded in paraffin, and sectioned at a thickness of 5 μm. The sections were deparaffinized and subjected to antigen retrieval, fol-

lowed by blocking of endogenous peroxidase activity. After blocking with BSA for 30 min, the sections were incubated overnight at 4 °C with primary antibodies against IL-1β, IL-6, IL-18, and TNF-α. After washing with PBS, the sections were incubated with the appropriate secondary antibody. Following further PBS washes, the sections were developed with DAB chromogenic solution, counterstained, dehydrated, and mounted. Images were acquired using a fluorescent microscope.

2.3.7 Detection of Positive Rates

Mouse myocardial tissue sections were deparaffinized and rehydrated, followed by microwave-assisted antigen retrieval in citrate buffer. The sections were washed three times with PBS and incubated with TUNEL reaction solution at 37 °C according to the manufacturer's instructions. After washing with PBS, the sections were treated with H_2O_2 and methanol to block endogenous peroxidase activity, followed by further PBS washing and DAB development. The sections were counterstained with hematoxylin, dehydrated, cleared, mounted, and observed and photographed using a light microscope.

2.3.8 Transmission Electron Microscopy

Mouse myocardial tissue samples measuring approximately 1 mm^3 were fixed in 1% osmium tetroxide prepared in phosphate buffer at room temperature. The samples were dehydrated through a graded ethanol series and infiltrated and embedded in a mixture of acetone and 812 embedding resin. Ultrathin sections (60 nm thick) were prepared and collected on 150-mesh copper grids. The sections were stained with 2% saturated alcoholic uranyl acetate, followed by staining with 2.6% lead citrate solution. The ultrastructure of myocardial tissue was examined and photographed using a transmission electron microscope (Hitachi, Japan).

2.3.9 Western Blot Analysis

Protein extraction and Western blot analysis were performed according to a previously described method [27]. PLIN5 and NLRP3 were detected using primary antibodies at 0.2 μg/mL (1:1000) and 0.548 μg/mL (1:1000), respectively. The expression of mitochondrial-associated PLIN5 in myocardial tissue was analyzed by Western blotting. The optical density of the protein bands was quantified using ImageJ software.

2.3.10 Quantitative Real-Time PCR Analysis of PLIN5 Expression

RNA extraction, reverse transcription, and quantitative real-time PCR (RT-qPCR) were performed according to a previously described method [27]. Relative mRNA expression levels were calculated using the $2^{-\Delta\Delta Cq}$ method, with β-actin used as the reference gene. The primer sequences were as follows: PLIN5 (Forward: 5′-ATGAGTCAAGCCATGGACATG-3′, Reverse: 5′-AAAGAGTGTTCATAGGCGAGAT-3′), and β-actin (Forward: 5′-GGCTGTATTCCCCTCCATCG-3′, Reverse: 5′-CCAGTTGGTAACAATGCCATGT-3′).

2.3.11 Identification of Mitochondrial-Related Proteins Among PLIN5-Interacting Proteins

Protein samples were subjected to reduction and enzymatic digestion after dilution of the enzyme solution with 25 mM NH_4HCO_3. Following gradient elution, the resulting peptide solutions were collected, frozen, and dried for further analysis. The samples were enriched and desalted. Peptide separation was performed using a column with an inner diameter of 75 μm, a particle size of 3 μm, and a length of 25 cm at a flow rate of 300 nL/min. The separated peptides were introduced into a tandem mass spectrometer and analyzed in data-dependent acquisition (DDA) mode using higher-energy collisional dissociation (HCD) for ion fragmentation. The acquired mass spectrometry data were matched against theoretical spectra generated from the corresponding protein database to identify proteins. GO and KOG functional annotation analyses were then performed. The intensity-based absolute quantification (iBAQ) value was calculated by dividing the total protein peak area by the number of theoretically observable peptides and was used as a measure of relative protein abundance.

2.4 In Vitro Experiments

2.4.1 Cell Culture and Grouping

H9c2 cell lines were validated by STR profiling and tested negative for mycoplasma. Cells were cultured in high-glucose DMEM supplemented with 10% fetal bovine serum (FBS) and 1% penicillin-streptomycin solution, in a 37 °C, 5% CO_2 incubator. H9c2 cells were randomly divided into three groups: the negative-control (NC) group, in which cells were transfected with the NC plasmid and cultured in complete medium for 24 h after transfection; the NC + palmitic acid (PA) group, in which cells were transfected with the NC plasmid and cultured for 24 h in complete medium containing 200 μmol/L PA; and the PA + PLIN5-OE group, in which cells were transfected with the PLIN5 overexpression plasmid and cultured for 24 h in complete medium containing 200 μmol/L PA.

2.4.2 Immunofluorescence Staining for Protein Detection

H9c2 cells were fixed with 4% paraformaldehyde for 20 min, permeabilized with 0.5% Triton X-100 for 20 min, and blocked with 10% goat serum for 1 h. The cells were then incubated overnight at 4 °C with primary antibodies against NLRP3, caspase-1, and GSDMD (1:200). After washing to remove unbound primary antibodies, the cells were incubated with Alexa Fluor 488-conjugated secondary antibodies (1:200) for 1 h and counterstained with DAPI. Fluorescence images were acquired, and fluorescence intensity was quantified using ImageJ software.

2.4.3 Immunofluorescence Detection of Lipid Peroxidation

H9c2 cells were treated with the lipid peroxidation probe BODIPY 581/591 C11 according to the manufacturer's instructions. Fluorescence images were acquired using an inverted fluorescence microscope.

2.4.4 Immunofluorescence Detection of ROS

H9c2 cells were incubated with 1 mL of ROS detection working solution at 37 °C for 30 min. The cells were then washed three times with serum-free medium, and fluorescence images were acquired using an inverted fluorescence microscope.

2.4.5 Hoechst assay for detecting pyroptosis of cells

After collecting the supernatant of H9c2 cells, they were washed twice with PBS. 1 mL of Hoechst33342 solution was added to each well, and incubated at 37 °C for 10 min. After discarding the Hoechst staining solution, they were washed twice with PBS, and 1 mL of PI solution was added to each well. The incubation was conducted in the dark at 37 °C for 10 min. Finally, the PI solution was discarded, and the cells were washed twice with PBS before imaging with a fluorescence microscope.

2.4.6 Oxygen Consumption Rate (OCR) for Detection of the Energy Metabolism Level

H9c2 cells were seeded into XFe96 cell culture plates, allowed to attach for 1 h, and cultured overnight. For sensor cartridge hydration, 200 µL of XF calibration solution was added to each well of the utility plate, and the sensor cartridge was placed on the plate and incubated overnight at 37 °C in a CO_2-free incubator. Following cell attachment, the cells were randomly assigned to the corresponding treatment groups and subjected to the indicated interventions for 24 h. Seahorse assay medium was prewarmed to 37 °C. The culture medium was aspirated, and the cells were washed once with 200 µL of assay medium. The wash medium was removed, and 160 µL of fresh assay medium was added to each well, resulting in a final volume of 180 µL per well. The plates were incubated at 37 °C in a CO_2-free incubator for 60 min before measurement. The designated compounds were loaded into the injection ports and sequentially injected according to the manufacturer's instructions. OCR was measured using the Seahorse XFe96 extracellular flux analyzer, and the data were analyzed using Wave Pro software.

2.4.7 Confocal Microscopy Analysis of LD–Mitochondrial Co-Localization

H9c2 cells in each experimental group were treated according to the corresponding experimental design and maintained at 37 °C in a humidified incubator containing 5% CO_2. Mitochondria were stained with a mitochondrial red fluorescent probe (200 nM) for 30 min at 37 °C. LDs were then stained with a lipid droplet fluorescent probe prepared by diluting the probe in lipid droplet detection buffer at a 1:1000 ratio and incubated for 15 min at 37 °C in a 5% CO_2 incubator. The cells were then washed and fixed with 4% paraformaldehyde for 20 min at 37 °C, followed by washing with PBS. Images were acquired using a Leica STELLARIS 5 confocal laser scanning microscope (Leica Microsystems, Germany).

2.5 Statistical Analysis

Statistical analyses were performed using GraphPad Prism 8.0. Data were analyzed using one-way analysis of variance (ANOVA), followed by Tukey's post hoc test. A p value < 0.05 was considered statistically significant.

3. Results

3.1 Successful Establishment of the Diabetic Myocardial Injury Model

Compared with the db/m group, body weight and serum levels of GLU, TC, TG, and LDL-C were significantly increased, whereas HDL-C levels were significantly decreased in the db/db group ($p < 0.01$; Fig. 1A–F). These findings confirmed the pathological characteristics of the diabetic mouse model. Histopathological examination revealed marked structural abnormalities in the myocardium of db/db mice. Compared with the db/m group, myocardial fibers in the db/db group were disorganized and exhibited a wavy appearance, with partial myofibrillar dissolution, cardiomyocyte hypertrophy, vacuolar degeneration, coagulative necrosis, and inflammatory cell infiltration. MASSON staining showed a significant increase in blue-stained areas within the myocardial interstitium and a higher proportion of collagen deposition in db/db mice than in db/m mice ($p < 0.01$), indicating pronounced myocardial fibrosis. WGA staining further showed an increased cardiomyocyte cross-sectional area in db/db mice, indicating cardiomyocyte hypertrophy (Fig. 1G–I). Cardiac function was assessed using M-mode echocardiography (Fig. 1G). Compared with the db/m group, both EF and FS were significantly decreased in db/db mice ($p < 0.01$; Fig. 1J,K), indicating impaired cardiac systolic function. The HW/TL ratio was also significantly higher in db/db mice than in db/m mice ($p < 0.01$; Fig. 1L), consistent with cardiac hypertrophy. db/db mice exhibited metabolic abnormalities accompanied by myocardial inflammation, cardiomyocyte injury and hypertrophy, fibrosis, and impaired systolic function at 16 weeks of age (Fig. 1M). These findings indicate that the db/db mouse model mimics key pathological features of diabetic myocardial injury and is suitable for further investigation of the underlying mechanisms.

3.2 Transcriptomic Analysis of Myocardial Tissue

Transcriptomic analysis identified 2576 DEGs in the myocardial tissues of db/db mice compared with db/m mice, including 1560 upregulated and 1016 downreg-

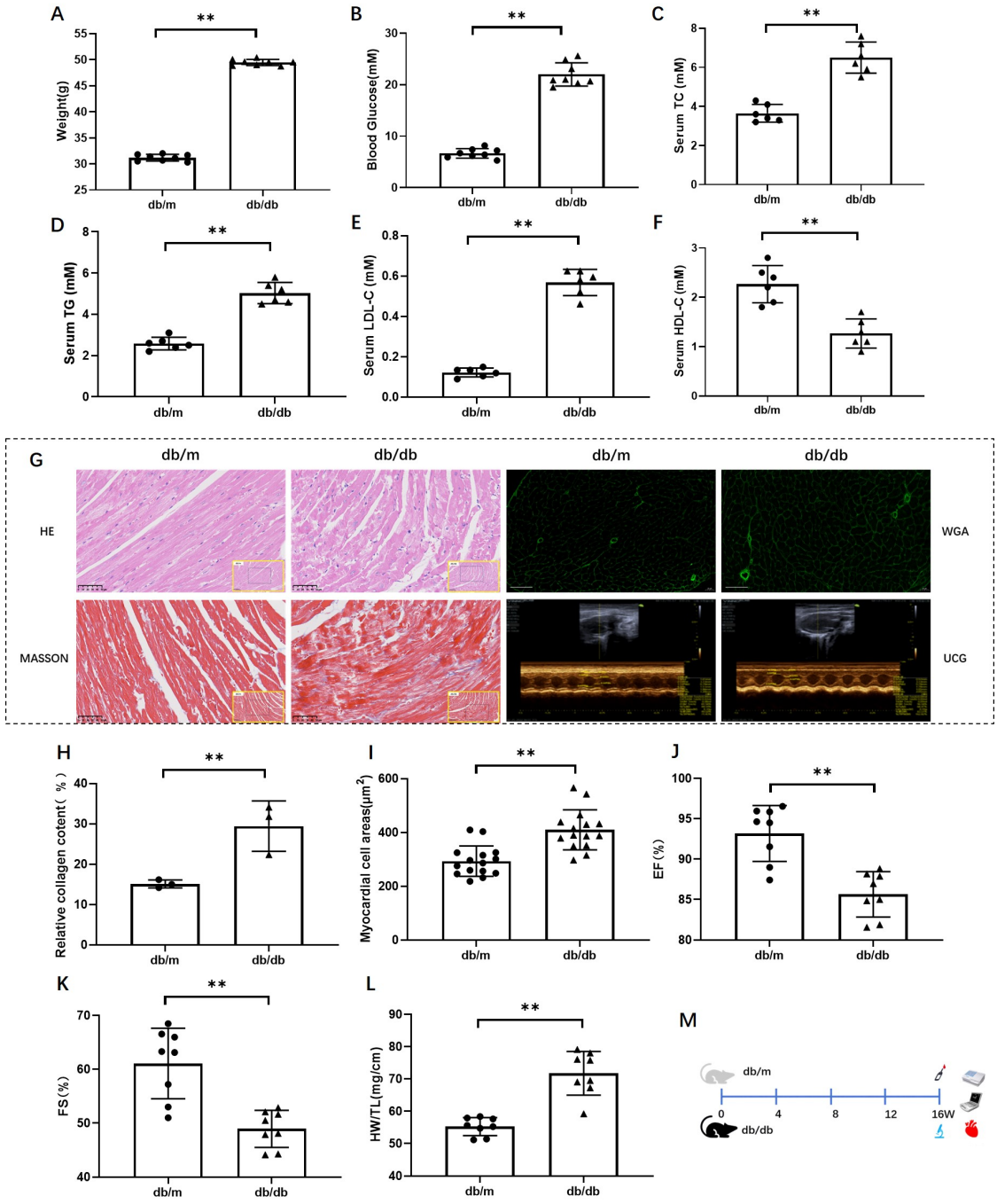

Fig. 1. The sign of successful modeling of myocardial injury. (A) Weight, (n = 8) (B) Blood glucose, (n = 8) (C) TC, (n = 6) (D) TG, (n = 6) (E) LDL-C, (n = 6) (F) HDL-C, (n = 6) (G) HE (Scale bar = 50 μm), MASSON (Scale bar = 50 μm), WGA (Scale bar = 20 μm) and UCG graphs, (H) Relative collagen content, (n = 3) (I) Myocardial cell areas, (n = 3) (J) EF, (n = 8) (K) FS, (n = 8) (L) HW/TL, (n = 8) (M) The time course of the mouse sample collection. Compared with db/m group, $^{**}p < 0.01$, TC, total cholesterol; TG, triglyceride; LDL-C, low-density lipoprotein cholesterol; HDL-C, high-density lipoprotein cholesterol; HE, Hematoxylin-eosin stain; MASSON, Masson trichrome stain; WGA, Wheat Germ Agglutinin stain; UCG, Ultrasound Cardiogram; EF, ejection fraction; FS, fractional shortening; HW/TL, heart weight-to-tibial length ratio.

ulated genes (Fig. 2A). KEGG enrichment analysis identified 20 significantly enriched pathways among the DEGs (Fig. 2B). The major enriched pathways included DCM, oxidative phosphorylation, thermogenesis, chemical carcinogenesis–reactive oxygen species, prion disease, Parkinson disease, amyotrophic lateral sclerosis, and Huntington disease. GO enrichment analysis identified 60 significantly enriched GO terms among the DEGs (Fig. 2C–

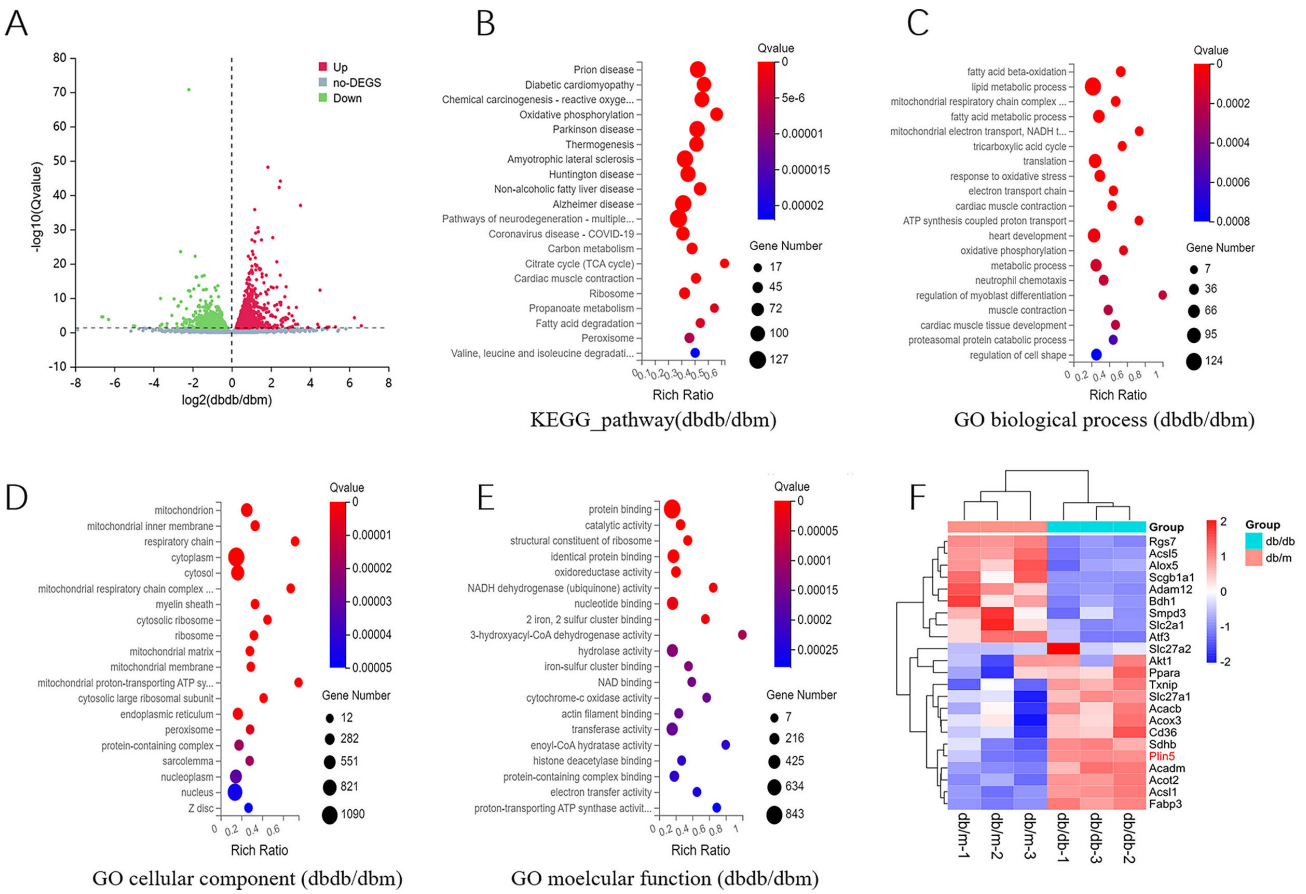

Fig. 2. Analysis of transcriptome sequencing results of myocardial tissue. (A) Differential gene map, (B) KEGG analysis, (C) BP analysis, (D) CC analysis, (E) MF analysis, (F) Heat map of differential genes. GO, Gene Ontology; KEGG, Kyoto Encyclopedia of Genes and Genomes; BP, Biological Process; CC, Cellular Component; MF, Molecular Function.

E). Given the involvement of lipid metabolic abnormalities and mitochondrial dysfunction in DCM, DEGs associated with lipid metabolism and mitochondrial function were further analyzed. A total of 23 DEGs showed differential expression between the myocardial tissues of db/m and db/db mice (Fig. 2F). The results showed that the top 5 differences included: fatty acid-binding protein 3 (FABP3), a member of the fatty acid-binding protein family that is highly expressed in cardiac tissue and can promote the uptake and transport of fatty acids by cells; Long-chain acyl-CoA synthetase 1 (ACSL1), located on the outer mitochondrial membrane, which catalyzes the formation of fatty acyl-CoA and participates in fatty acid metabolism; Medium-chain acyl-CoA dehydrogenase (ACADM), a mitochondrial enzyme involved in the β-oxidation of medium-chain fatty acids; acyl-CoA thioesterase 2 (ACOT2), located within mitochondria which hydrolyzes fatty acyl-CoA and participates in lipid metabolism and cellular energy homeostasis; and PLIN5, a LD-associated protein that is highly expressed in the heart. Among the lipid metabolism- and mitochondria-related genes, FABP3, ACSL1, ACADM, ACOT2, and PLIN5 showed prominent differential expression.

3.3 Changes in Inflammatory Factors and Pyroptosis-Related Markers in Myocardial Tissue

Immunohistochemical analysis showed the expression of IL-1β, IL-6, IL-18, and TNF-α in myocardial tissue (Fig. 3A,C–F). Compared with the db/m group, the areas of brown staining for IL-1β, IL-6, IL-18, and TNF-α were significantly increased in the db/db group ($p < 0.05$ or $p < 0.01$). NLRP3 protein expression in myocardial tissue was also significantly higher in db/db mice than in db/m mice ($p < 0.05$; Fig. 3B). TUNEL staining showed an increased proportion of TUNEL-positive cells in the myocardial tissue of db/db mice compared with db/m mice ($p < 0.01$; Fig. 3G). Because TUNEL staining detects DNA fragmentation, the increased TUNEL-positive rate indicates enhanced cardiomyocyte cell death in the db/db group. Together with the increased expression of NLRP3 and inflammatory cytokines, these findings suggest increased activation of inflammatory and pyroptosis-related pathways in the myocardium of diabetic mice.

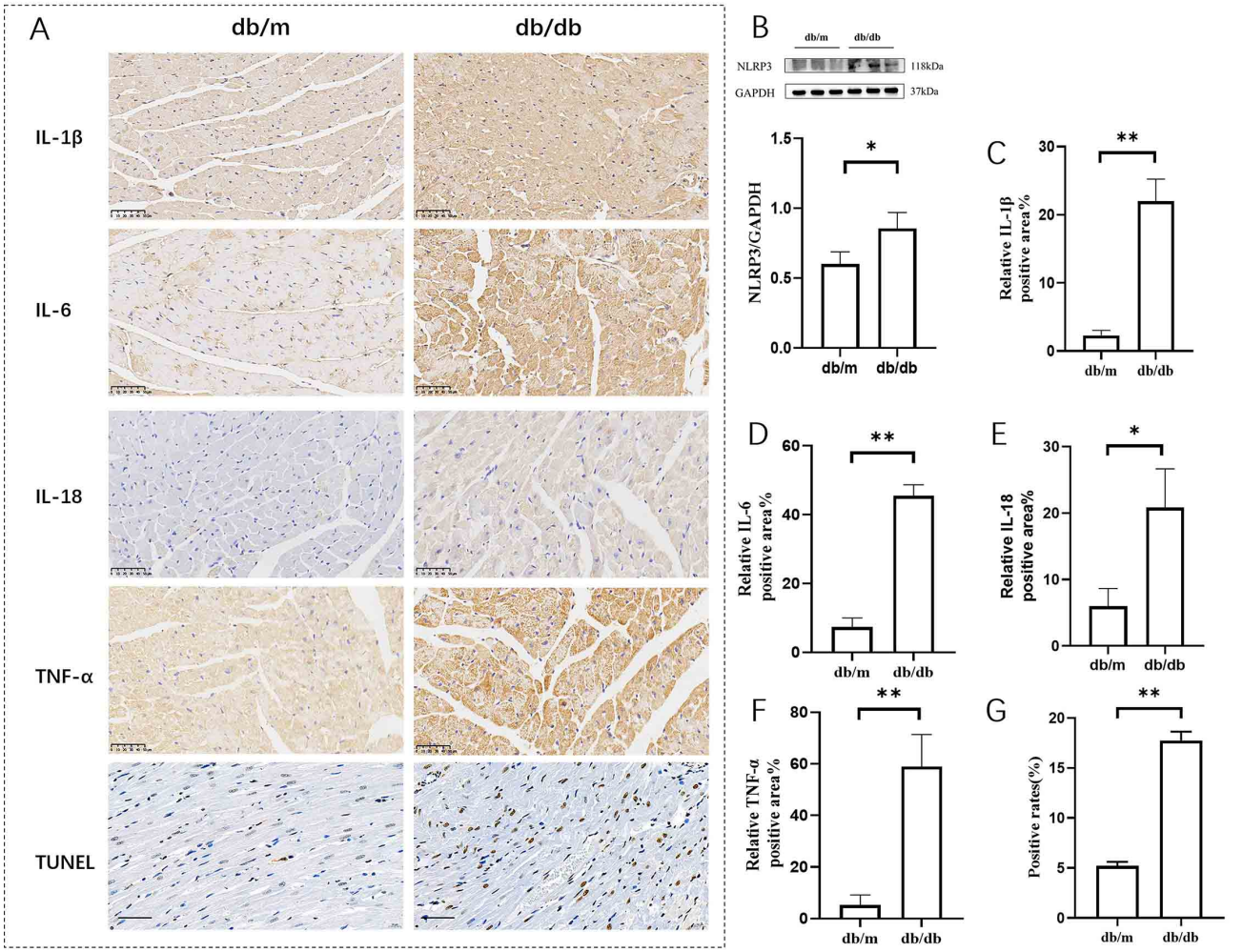

Fig. 3. Changes in inflammatory factors and pyroptosis in myocardial tissue. (A) Immunohistochemical images of IL-1β, IL-6, IL-18 and TNF-α, and image of TUNEL, (B) NLRP3 protein, (C) IL-1β positive area, (D) IL-6 positive area, (E) IL-18 positive area, (F) TNF-α positive area, (G) Positive rates. Compared with db/m group, $^{*}p < 0.05$, $^{**}p < 0.01$. NLRP3, Nucleotide-binding oligomerization domain, leucine-rich repeat and pyrin domain-containing 3. Scale bar = 50 μm.

3.4 Lipid Deposition, LD–Mitochondrial Distribution, and PLIN5 Expression in Myocardial Tissue

Oil Red O staining showed only a small number of red LDs in the myocardial tissue of db/m mice, whereas numerous red-stained LDs were distributed throughout the myocardial tissue of db/db mice. In the myocardial tissues of the db/m group mice, only a few red particles were observed; while in the myocardial tissues of the db/db mice, red particles were widely distributed (Fig. 4A), indicating marked myocardial lipid accumulation. Transmission electron microscopy revealed well-organized myocardial fibers, a small number of LDs, intact mitochondrial membranes, and clearly defined mitochondrial cristae in the db/m group. Mitochondria were frequently observed adjacent to LDs, with direct contacts between the two organelles. In db/db mice, myocardial fibers were disorganized, and a large number of LDs were present. Mitochondria exhibited swelling, membrane damage, loss of cristae, and vacuolar changes. Although mitochondria were distributed around LDs, direct LD–mitochondrial contacts were rarely observed (Fig. 4B). Lipid metabolism disorder can cause significant LD deposition in myocardial tissue, interfere with the contact between LDs and mitochondria, inhibit the interaction between LDs and mitochondria, and induce mitochondrial damage. Total protein was extracted from myocardial tissue. Western blot and qRT-PCR analyses showed that total PLIN5 protein and *PLIN5* mRNA expression in myocardial tissue were significantly increased in db/db mice compared with db/m mice ($p < 0.01$; Fig. 4C,D). These findings were consistent with the transcriptomic analysis and indicated increased overall PLIN5 expression in diabetic myocardial tissue. However, mitochondrial PLIN5 protein expression was significantly decreased in db/db mice compared with db/m mice ($p < 0.01$; Fig. 4E). Thus, diabetic myocardial tissue exhibited marked lipid accumulation, mitochondrial structural abnormalities,

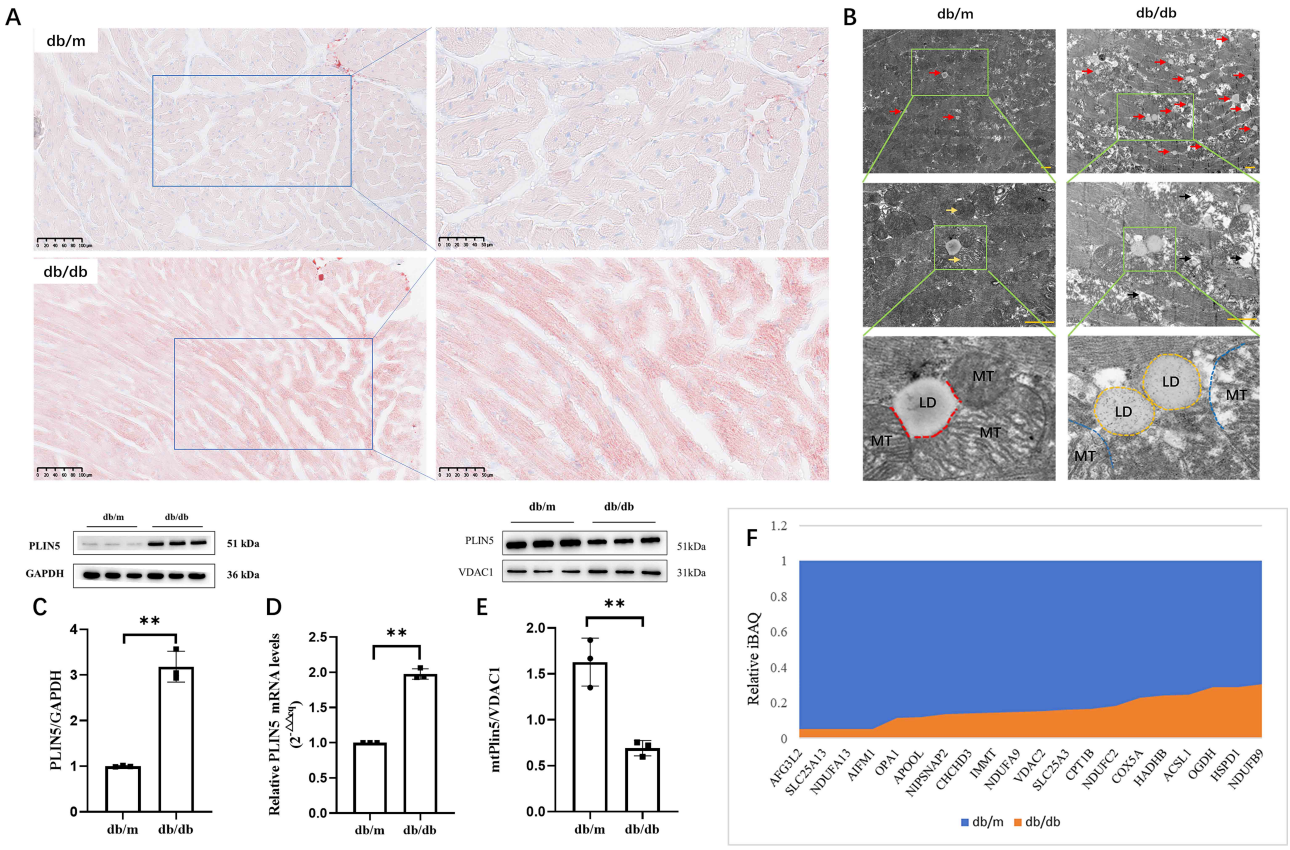

Fig. 4. Lipid deposition, lipid droplet and mitochondrial distribution, and PLIN5 protein expression. (A) Oil red O staining (left, scale bar = 100 μm; right, scale bar = 50 μm), (B) Electron microscopic observation, scale bar = 1 μm, (C) The protein expression of PLIN5 in total protein, (D) The gene expression of PLIN5 in total protein, (E) The protein expression of PLIN5 in mitochondria, (F) Analysis of the relative expression level of iBAQ. Compared with db/m group, $^{**}p < 0.01$. Red arrow: lipid droplet; Yellow arrow: structurally complete mitochondria; Black arrow: structurally damaged mitochondria; Yellow dotted line: lipid droplet membrane; Blue dotted line: mitochondrial membrane; Red dotted line: contact site between lipid droplet and mitochondria; LD, lipid droplet; MT, mitochondria; PLIN5, Perilipin 5; iBAQ, intensity-based absolute quantification.

increased total PLIN5 protein and gene expression, and reduced mitochondrial-associated PLIN5 expression. These findings suggest that the redistribution of PLIN5 may be associated with impaired LD–mitochondrial interactions during diabetic myocardial injury. Based on the relative iBAQ expression levels, the 20 mitochondrial-associated proteins showing the most pronounced differences were further analyzed. The expression levels of AFG3L2, SLC25A13, NDUFA13, AIFM1, OPA1, APOOL, NIPSNAP2, CHCHD3, IMMT, NDUFA9, VDAC2, SLC25A3, CPT1B, NDUFC2, COX5A, HADHB, ACSL1, OGDH, HSPD1, and NDUFB9 were decreased (Fig. 4F). These findings indicate that multiple mitochondrial-associated proteins among the PLIN5-interacting protein profile were reduced in db/db myocardial tissue, supporting impaired LD–mitochondrial interactions in DCM.

3.5 Effects of PLIN5 Overexpression on Pyroptosis in H9c2 Cardiomyocytes

Compared with the NC group, pyroptosis was significantly increased in the PA group ($p < 0.01$). PLIN5 overexpression significantly reduced pyroptosis compared with the PA group ($p < 0.01$; Fig. 5A,B). These findings indicate that PLIN5 overexpression attenuated PA-induced pyroptotic cell death in H9c2 cardiomyocytes. Compared with the NC group, the protein and mRNA expression levels of NLRP3, caspase-1, and GSDMD were significantly increased in the PA group ($p < 0.01$). PLIN5 overexpression significantly reduced the expression of these pyroptosis-related proteins and genes compared with the PA group ($p < 0.01$; Fig. 5C–K). These results indicate that PLIN5 overexpression suppresses PA-induced NLRP3/caspase-1/GSDMD pyroptosis in H9c2 cardiomyocytes.

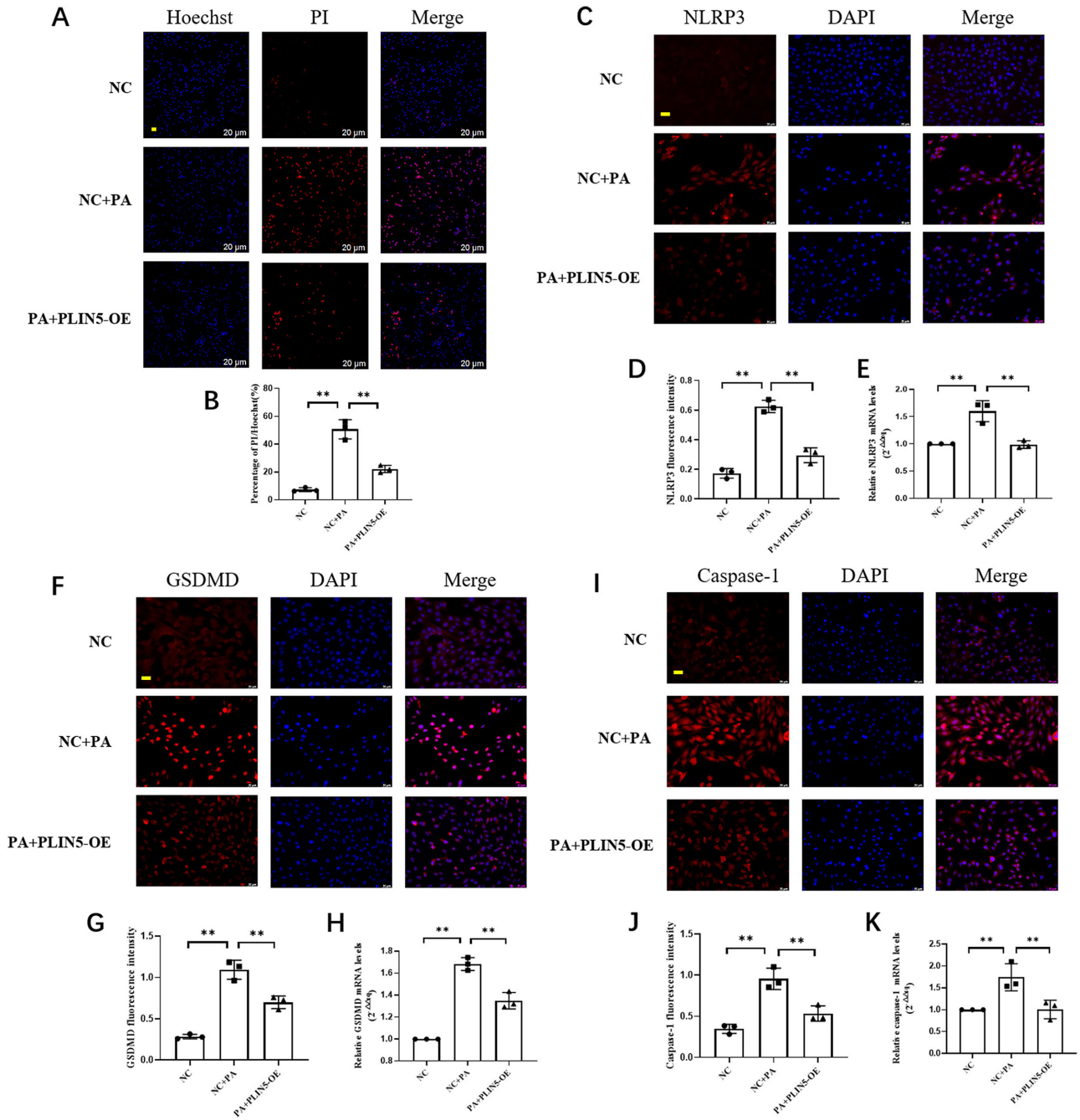

Fig. 5. Effects of PLIN5 overexpression on pyroptosis in H9c2 cardiomyocytes. (A) Immunofluorescence of pyroptosis, scale bar = 20 μm, (B) pyroptosis level, (C) Immunofluorescence of NLRP3, scale bar = 50 μm, (D) NLRP3 fluorescence intensity, (E) NLRP3 mRNA, (F) Immunofluorescence of GSDMD, scale bar = 50 μm, (G) GSDMD fluorescence intensity, (H) GSDMD mRNA, (I) Immunofluorescence of Caspase-1, (J) Caspase-1 fluorescence intensity, scale bar = 50 μm, (K) Caspase-1 mRNA. Compared with PA group, $^{**}p < 0.01$. NC, negative-control; PA, palmitic acid; OE, Over Expression; GSDMD, gasdermin D.

3.6 Effects of PLIN5 Overexpression on Lipid Peroxidation, ROS Production, Mitochondrial Respiration, and LD–Mitochondrial Co-Localization

Lipid peroxidation was assessed using the BODIPY 581/591 C11 lipid peroxidation probe. During lipid peroxidation, the fluorescence signal shifts from red to green, and the relative fluorescence intensities can be used to assess the extent of lipid peroxidation. Compared with the PA group, PLIN5 overexpression significantly decreased the lipid peroxidation level ($p < 0.01$; Fig. 6A,B), indicating that PLIN5 decreased PA-induced lipid peroxidation in H9c2 cardiomyocytes. ROS levels were also significantly lower in the PLIN5-OE group than in the PA group ($p < 0.01$; Fig. 6C,D). These findings indicate that

PLIN5 overexpression reduced PA-induced ROS accumulation and oxidative stress in H9c2 cardiomyocytes. Cellular oxygen consumption was measured using an Agilent Seahorse XFe96 analyzer. The basal OCR of the NC group represents mitochondrial oxygen consumption under basal conditions, whereas the maximal OCR measured after mitochondrial uncoupling reflects the maximal respiratory capacity of the cells under normal conditions. After the addition of a mitochondrial uncoupling agent for oxidative phosphorylation, OCR reaches its maximum, indicating total mitochondrial oxygen consumption under stress conditions. Compared with the PA group, maximal OCR was significantly decreased in the PLIN5-OE group ($p < 0.05$; Fig. 6E–G). These findings indicate that PA altered mitochondrial respiratory function in H9c2 cardiomyocytes and that PLIN5 overexpression affected the mitochondrial respiratory response to PA treatment. For co-localization analysis, LDs were labeled with green fluorescence and mitochondria with red fluorescence. In the NC group, a relatively small number of LDs were observed, whereas mitochondria were widely and uniformly distributed throughout the cells. PA treatment increased LD accumulation, but did not produce a corresponding increase in LD–mitochondrial co-localization. Overexpression of PLIN5 leads to a significant co-localization of mitochondria and lipid droplets (Fig. 6H). These findings suggest that PLIN5 overexpression promotes the spatial association of LDs with mitochondria in PA-treated H9c2 cardiomyocytes.

4. Discussion

DCM is a distinct cardiac complication of diabetes that often develops insidiously and may remain clinically asymptomatic during the early stage. The pathological features of DCM involve changes at the cellular, molecular, and structural levels, including cardiomyocyte hypertrophy, myocardial fibrosis, inflammatory cell infiltration, mitochondrial structural and functional abnormalities, impaired myocardial energy metabolism, and increased availability of FFAs [28]. As the disease progresses, left ventricular mass and ventricular wall thickness increase, accompanied by diastolic dysfunction and a gradual decline in systolic reserve. In advanced DCM, cardiomyocyte apoptosis and necrosis become more prominent, accompanied by diffuse myocardial fibrosis. Progressive diastolic dysfunction may eventually lead to impaired systolic function, reduced ejection fraction, and HF [29,30].

The pathogenesis of DCM is complex and involves metabolic, inflammatory, oxidative, and mitochondrial abnormalities. Clinical evidence indicates that intensive glycemic control alone may not adequately prevent cardiovascular complications in patients with diabetes [31]. Abnormal lipid metabolism is an important contributor to DCM. Increased circulating FFAs promote excessive myocardial fatty acid uptake, and when lipid uptake exceeds the capacity for oxidation and storage, excess lipids accumulate within cardiomyocytes and induce lipotoxicity. This metabolic imbalance can disrupt intracellular organelle function and promote inflammation, oxidative stress, and impaired energy metabolism, ultimately contributing to cardiomyocyte apoptosis, necrosis, pyroptosis, and ferroptosis and promoting pathological myocardial remodeling and HF [32,33]. Therefore, investigating DCM from the perspective of lipid metabolic dysregulation may provide new insights into its pathogenesis and therapeutic strategies.

LDs are dynamic organelles with a variety of characteristics and roles that participate in energy storage, lipid metabolism, metabolic signaling, intracellular lipid and membrane transport, and inflammatory responses [34,35]. Mitochondria are also two important regulators of cellular energy metabolism, and functional interactions between LDs and mitochondria contribute to lipid storage, lipid utilization, and energy production [26,36]. Physical contacts between LDs and mitochondria facilitate the transfer of fatty acids and other metabolites between these organelles and can affect both LD metabolism and mitochondrial fatty acid oxidation [37,38]. Dysregulation of these interactions may therefore affect lipid metabolism, mitochondrial function, lipid peroxidation, and oxidative stress, potentially contributing to inflammatory injury and pyroptosis.

Perilipins, also known as the PAT proteins, are LD-associated proteins that comprise five major members, PLIN1–PLIN5. PLIN5 is highly expressed in metabolically active tissues, including the heart, liver, and skeletal muscle [39]. PLIN5 contributes to LD formation and lipid storage and has been implicated in regulating LD–mitochondrial interactions [40]. The regulatory role of PLIN5 in the interaction between LDs and mitochondria is reflected in lipid metabolism. PLIN5 can inhibit LD hydrolysis, promote TG generation from fatty acids and their storage in LDs, down-regulate the expression of carnitine palmitoyltransferase and mitochondrial oxidation-related genes, and limit β-oxidation of fatty acids [41]. The C-terminal region of PLIN5 can also participate in mitochondrial recruitment to LDs, facilitating the transfer and utilization of fatty acids and potentially limiting the accumulation of cytotoxic lipid species [32]. Therefore, elucidating how the PLIN5-regulated LD–mitochondrial pathway mediates lipid metabolism and transport and influences mitochondrial energy metabolism is important for understanding the physiological functions of LDs and clarifying the role of LD–mitochondrial interactions in the pathogenesis of DCM.

In this study, db/db mice, a well-established T2DM model characterized by insulin resistance and abnormal blood glucose and blood lipids, were used to study cardiovascular complications of diabetes. Assessment of cardiac mass index, HE, MASSON, and WGA staining, together with echocardiographic analysis, demonstrated cardiomyocyte hypertrophy, myocardial fibrosis, inflamma-

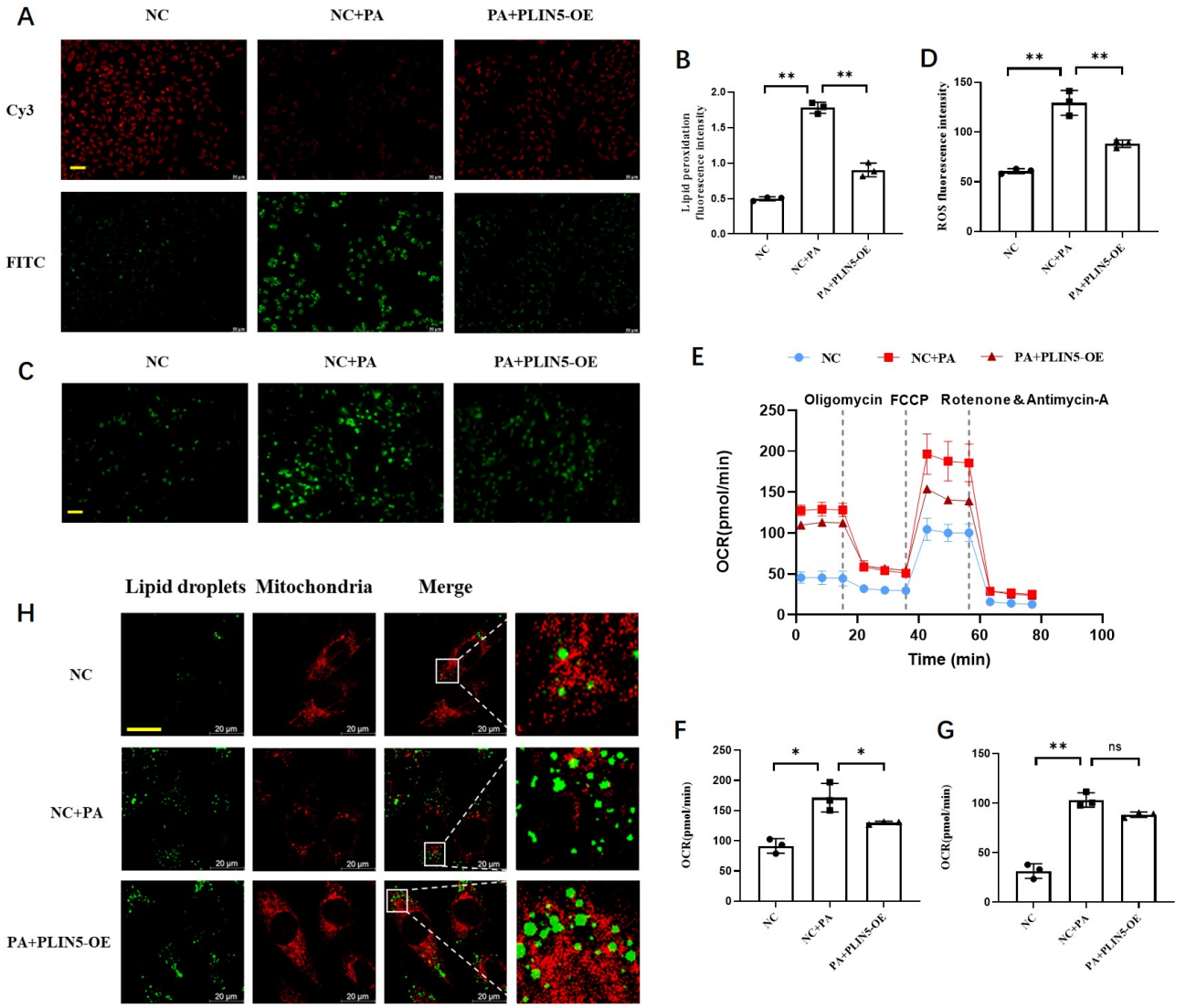

Fig. 6. Effects of PLIN5 overexpression on lipid peroxidation, ROS production, mitochondrial respiration, and LD–mitochondrial co-localization in H9c2 cardiomyocytes. (A) Lipid peroxidation fluorescence graph, scale bar = 50 μm. (B) Lipid peroxidation fluorescence intensity, (C) ROS fluorescence graph, scale bar = 50 μm, (D) ROS fluorescence intensity, (E) OCR detection of cells in each group, (F) Maximum OCR analysis, (G) Basal OCR analysis, (H) Co-localization analysis of LDs and mitochondria, scale bar = 20 μm. Compared with PA group, ns, non-significant, $^{*}p < 0.05$, $^{**}p < 0.01$. ROS, reactive oxygen species; OCR, oxygen consumption rate; LDs, lipid droplets.

tory infiltration, myocardial injury, and impaired systolic function, as reflected by reduced EF and FS. The results demonstrated that db/db mice exhibited key pathological features of DCM, confirming the successful establishment of the diabetic myocardial injury model. Transcriptomic analysis further showed significant upregulation of FABP3, ACSL1, ACADM, ACOT2, and PLIN5 in the myocardial tissue of db/db mice. These findings highlight the importance of abnormal lipid metabolism, myocardial lipid accumulation, and mitochondrial dysfunction in the pathogenesis of diabetic myocardial injury. Electron microscopy and fluorescence imaging revealed marked LD accumulation and mitochondrial damage in the myocardium of diabetic mice, accompanied by altered LD–mitochondrial co-localization. These findings suggest that disruption of LD–mitochondrial interactions may be associated with mitochondrial injury under conditions of abnormal lipid metabolism. Furthermore, NLRP3 expression and the levels of IL-1β, IL-6, IL-18, and TNF-α were increased in the myocardial tissue of db/db mice, indicating activation of inflammatory pathways. The elevated levels of these inflammatory mediators are consistent with the chronic inflammatory state reported in patients with diabetes and its complications [42,43,44]. Persistent inflammatory activation may contribute to myocardial injury and pathological remodeling in DCM. These findings suggest that ab-

normal lipid metabolism and myocardial lipid accumulation are important contributors to diabetic myocardial injury and that impaired LD–mitochondrial interactions may be associated with mitochondrial dysfunction and inflammatory responses. Pyroptosis-related changes may represent an important component of diabetic myocardial injury, although further mechanistic studies are required to establish whether LD–mitochondrial dysfunction directly drives cardiomyocyte pyroptosis.

To further investigate the potential role of PLIN5, a PA-induced lipotoxicity model was established in H9c2 cardiomyocytes, followed by PLIN5 overexpression. PA treatment promoted LD accumulation, increased lipid peroxidation and ROS production, altered mitochondrial respiratory function, reduced LD–mitochondrial co-localization, and increased pyroptosis-related markers. Overexpression of PLIN5 can significantly promote the interaction between LDs and mitochondria, improve mitochondrial function, and inhibit pyroptosis. These findings support a potential role for PLIN5-mediated LD–mitochondrial interactions in the pathogenesis of DCM. Disruption of these interactions under conditions of abnormal lipid metabolism may contribute to lipid accumulation, mitochondrial dysfunction, oxidative stress, and pyroptosis-related signaling. The PLIN5-regulated LD–mitochondrial pathway may therefore represent a potential mechanism linking myocardial lipid metabolic dysregulation with pyroptosis in DCM and warrants further investigation as a therapeutic target.

5. Limitations

This study demonstrated that diabetes is associated with disrupted LD–mitochondrial co-localization in cardiomyocytes and identified PLIN5 as a potential regulator of this process. Several mitochondrial-associated proteins were further identified that showed altered abundance among the PLIN5-associated protein profile. However, the molecular mechanism by which PLIN5 regulates LD–mitochondrial contact remains unclear. Whether the identified mitochondrial proteins directly participate in PLIN5-mediated LD–mitochondrial interactions requires further validation. Furthermore, the specific molecular components responsible for establishing and regulating LD–mitochondrial contact and whether LD–mitochondrial contact regulates cellular signaling beyond lipid transfer have not been fully characterized. Further studies using targeted protein–protein interaction assays, genetic manipulation, and functional validation are required to elucidate these mechanisms.

6. Conclusion

Abnormal lipid metabolism and myocardial lipid accumulation are closely associated with diabetic myocardial injury. Lipid metabolic dysregulation, mitochondrial dysfunction, and oxidative stress may contribute to the development of DCM. This study identifies the PLIN5-regulated LD–mitochondrial pathway as a potential mechanism linking lipid metabolic dysregulation with myocardial injury and provides a basis for further investigation of its role in DCM.

Availability of Data and Materials

The datasets and raw data used and analyzed during the current study are available from the corresponding authors upon request.

Author Contributions

PZ and HS designed the research study. LW and JYL performed the research. CZZ and HMD conducted experiments. ZQH analyzed the data. LW and JYL wrote the initial draft. All authors contributed to editorial changes in the manuscript. All authors read and approved the final manuscript. All authors have participated sufficiently in the work and agreed to be accountable for all aspects of the work.

Ethics Approval and Consent to Participate

This experiment was approved by the Laboratory Animal Ethics Committee of the Animal Research Committee of Anhui University of Chinese Medicine (AHUCM-mouse-2022031). The animal study was conducted in accordance with the ARRIVE guidelines 2.0 and National Institutes of Health (NIH) Guide for the Care and Use of Laboratory Animals.

Acknowledgment

The Graphical Abstract was created using BioGDP (https://biogdp.com).

Funding

This work was supported by the Young and middle-aged teachers training action project in Anhui Provincial Department of Education (DTR2023025), Key Project Foundation of Natural Science Research in Universities of Anhui Province (2024AH051041), and the foundation of Anhui Provincial Key Laboratory of Chinese Medicinal Formula (2024AKLCMF03).

Conflicts of Interest

The authors declare no conflicts of interest.

Supplementary Material

Supplementary material associated with this article can be found, in the online version, at https://doi.org/10.31083/FBL54145.

References

[1] Chung WK, Erion K, Florez JC, Hattersley AT, Hivert MF, Lee CG, et al. Precision Medicine in Diabetes: A Consensus Report From the American Diabetes Association (ADA) and the Eu-

ropean Association for the Study of Diabetes (EASD). Diabetes Care. 2020; 43: 1617–1635. https://doi.org/10.2337/dci20-0022
[2] Sun H, Saeedi P, Karuranga S, Pinkepank M, Ogurtsova K, Duncan BB, et al. IDF Diabetes Atlas: Global, regional and country-level diabetes prevalence estimates for 2021 and projections for 2045. Diabetes Research and Clinical Practice. 2022; 183: 109119. https://doi.org/10.1016/j.diabres.2021.109119
[3] Chan JCN, Lim LL, Wareham NJ, Shaw JE, Orchard TJ, Zhang P, et al. The Lancet Commission on diabetes: using data to transform diabetes care and patient lives. Lancet (london, England). 2021; 396: 2019–2082. https://doi.org/10.1016/S0140-6736(20)32374-6
[4] Jorsal A, Wiggers H, McMurray JJV. Heart Failure: Epidemiology, Pathophysiology, and Management of Heart Failure in Diabetes Mellitus. Endocrinology and Metabolism Clinics of North America. 2018; 47: 117–135. https://doi.org/10.1016/j.ecl.2017.10.007
[5] Kim AH, Jang JE, Han J. Current status on the therapeutic strategies for heart failure and diabetic cardiomyopathy. Biomedicine & Pharmacotherapy = Biomedecine & Pharmacotherapie. 2022; 145: 112463. https://doi.org/10.1016/j.biopha.2021.112463
[6] Januzzi JL, Del Prato S, Rosenstock J, Butler J, Ezekowitz J, Ibrahim NE, et al. Characterizing diabetic cardiomyopathy: baseline results from the ARISE-HF trial. Cardiovascular Diabetology. 2024; 23: 49. https://doi.org/10.1186/s12933-024-02135-z
[7] Jia G, Whaley-Connell A, Sowers JR. Diabetic cardiomyopathy: a hyperglycaemia- and insulin-resistance-induced heart disease. Diabetologia. 2018; 61: 21–28. https://doi.org/10.1007/s00125-017-4390-4
[8] Liu M, Chen P, Wang S, Zeng G, Lv Z. Adropin Alleviates High-Glucose-Induced Cardiomyocyte Apoptosis In Vitro via the Modulation of Mitophagy and Mitochondrial Dynamics. International Journal of Pharmacology. 2025; 21: 46592. https://doi.org/10.31083/ijp46592
[9] Liu P, Zhang Z, Chen H, Chen Q. Pyroptosis: Mechanisms and links with diabetic cardiomyopathy. Ageing Research Reviews. 2024; 94: 102182. https://doi.org/10.1016/j.arr.2023.102182
[10] Hao J, Zhou J, Hu S, Zhang P, Wu H, Yang J, et al. RTA 408 ameliorates diabetic cardiomyopathy by activating Nrf2 to regulate mitochondrial fission and fusion and inhibiting NF-κB-mediated inflammation. American Journal of Physiology. Cell Physiology. 2024; 326: C331–C347. https://doi.org/10.1152/ajpcell.00467.2023
[11] Greenwell AA, Gopal K, Ussher JR. Myocardial Energy Metabolism in Non-ischemic Cardiomyopathy. Frontiers in Physiology. 2020; 11: 570421. https://doi.org/10.3389/fphys.2020.570421
[12] Chinese Medical Doctor Association Endocrinology and Metabolism Physician Branch; Cardiovascular Metabolism Medicine Professional Committee of National Center for Cardiovascular Diseases. Expert consensus on the lipid management of diabetic patients (2024 Edition). Chinese Circulation Journal. 2024; 39: 322–341. https://doi.org/10.3969/j.issn.1000-3614.2024.04.002
[13] Wu M, Tan J, Cao Z, Cai Y, Huang Z, Chen Z, et al. Sirt5 improves cardiomyocytes fatty acid metabolism and ameliorates cardiac lipotoxicity in diabetic cardiomyopathy via CPT2 desuccinylation. Redox Biology. 2024; 73: 103184. https://doi.org/10.1016/j.redox.2024.103184
[14] Da Dalt L, Cabodevilla AG, Goldberg IJ, Norata GD. Cardiac lipid metabolism, mitochondrial function, and heart failure. Cardiovascular Research. 2023; 119: 1905–1914. https://doi.org/10.1093/cvr/cvad100
[15] Avagimyan A, Fogacci F, Pogosova N, Kakrurskiy L, Kogan E, Urazova O, et al. Diabetic Cardiomyopathy: 2023 Update by the International Multidisciplinary Board of Experts. Current Problems in Cardiology. 2024; 49: 102052. https://doi.org/10.1016/j.cpcardiol.2023.102052
[16] Stratmann B, Eggers B, Mattern Y, de Carvalho TS, Marcus-Alic K, Tschoepe D. Maladaptive response following glucose overload in GLUT4-overexpressing H9C2 cardiomyoblasts. Diabetes, Obesity & Metabolism. 2024; 26: 2379–2389. https://doi.org/10.1111/dom.15553
[17] Villa E, Saso L, Chichiarelli S, Rojas-Solé C, Pinilla-González V, Prieto JC, et al. Antioxidant Cardioprotection in Acute Myocardial Infarction: From Mechanisms to Therapeutic Strategies. Frontiers in Bioscience (landmark Edition). 2025; 30: 27678. https://doi.org/10.31083/FBL27678
[18] Panou T, Gouveri E, Rizzo M, Popovic DS, Papanas N. Ferroptosis and pyroptosis in diabetes mellitus: emerging therapeutic potential of GLP-1 receptor agonists. Frontiers in Clinical Diabetes and Healthcare. 2025; 6: 1657710. https://doi.org/10.3389/fcdhc.2025.1657710
[19] Tian Z, Cao Y, Liu J, Zheng X, Li J, Zhao J, et al. Metabolic pathways and cell death modalities in diabetic complications: unraveling pyroptosis, ferroptosis, cuproptosis, and disulfidptosis. Cell Death Discovery. 2026; 12: 307. https://doi.org/10.1038/s41420-026-03162-3
[20] Lu Y, Lu Y, Meng J, Wang Z. Pyroptosis and Its Regulation in Diabetic Cardiomyopathy. Frontiers in Physiology. 2022; 12: 791848. https://doi.org/10.3389/fphys.2021.791848
[21] Ding L, Yin J, Xu X, Xie D, Xiang D, Tong P, et al. Bufalin alleviates acute kidney injury by regulating NLRP3 inflammasome-mediated pyroptosis. Apoptosis: an International Journal on Programmed Cell Death. 2023; 28: 539–548. https://doi.org/10.1007/s10495-023-01815-7
[22] Wang F, Wang J, Liang X, Wu Z, Xue J, Yin L, et al. Ghrelin inhibits myocardial pyroptosis in diabetic cardiomyopathy by regulating ERS and NLRP3 inflammasome crosstalk through the PI3K/AKT pathway. Journal of Drug Targeting. 2024; 32: 148–158. https://doi.org/10.1080/1061186X.2023.2295268
[23] Li Y, Guo B. GSDMD-mediated pyroptosis: molecular mechanisms, diseases and therapeutic targets. Molecular Biomedicine. 2025; 6: 11. https://doi.org/10.1186/s43556-025-00249-8
[24] Petan T. Lipid Droplets in Cancer. Reviews of Physiology, Biochemistry and Pharmacology. 2023; 185: 53–86. https://doi.org/10.1007/112_2020_51
[25] Hu L, Tang D, Qi B, Guo D, Wang Y, Geng J, et al. Mfn2/Hsc70 Complex Mediates the Formation of Mitochondria-Lipid Droplets Membrane Contact and Regulates Myocardial Lipid Metabolism. Advanced Science (weinheim, Baden-Wurttemberg, Germany). 2024; 11: e2307749. https://doi.org/10.1002/advs.202307749
[26] Cui L, Liu P. Two Types of Contact Between Lipid Droplets and Mitochondria. Frontiers in Cell and Developmental Biology. 2020; 8: 618322. https://doi.org/10.3389/fcell.2020.618322
[27] Zhao CZ, Ding HM, Hu ZQ, Zhou L, Du YQ, Zhou P, et al. Exploring the mechanism of Ling-Gui-Zhu-Gan decoction in metabolic cardiomyopathy via inhibiting ferroptosis. Phytomedicine: International Journal of Phytotherapy and Phytopharmacology. 2024; 135: 156234. https://doi.org/10.1016/j.phymed.2024.156234
[28] Bellemare M, Bourcier L, Iglesies-Grau J, Boulet J, O'Meara E, Bouabdallaoui N. Mechanisms of diabetic cardiomyopathy: Focus on inflammation. Diabetes, Obesity & Metabolism. 2025; 27: 2326–2338. https://doi.org/10.1111/dom.16242
[29] Fang T, Wang J, Sun S, Deng X, Xue M, Han F, et al. JinLiDa granules alleviates cardiac hypertrophy and inflammation in diabetic cardiomyopathy by regulating TP53. Phytomedicine: International Journal of Phytotherapy and Phytopharmacology. 2024; 130: 155659. https://doi.org/10.1016/j.

phymed.2024.155659
[30] Rajbhandari J, Fernandez CJ, Agarwal M, Yeap BXY, Pappachan JM. Diabetic heart disease: A clinical update. World Journal of Diabetes. 2021; 12: 383–406. https://doi.org/10.4239/wjd.v12.i4.383
[31] Nathan DM, Lachin JM, Bebu I, Burch HB, Buse JB, et al. Glycemia Reduction in Type 2 Diabetes - Microvascular and Cardiovascular Outcomes. The New England Journal of Medicine. 2022; 387: 1075–1088. https://doi.org/10.1056/NEJMoa2200436
[32] Bodenstab ML, Varghese RT, Iacobellis G. Cardio-Lipotoxicity of Epicardial Adipose Tissue. Biomolecules. 2024; 14: 1465. https://doi.org/10.3390/biom14111465
[33] Tokarek J, Budny E, Saar M, Stańczak K, Wojtanowska E, Młynarska E, et al. Molecular Processes Involved in the Shared Pathways between Cardiovascular Diseases and Diabetes. Biomedicines. 2023; 11: 2611. https://doi.org/10.3390/biomedicines11102611
[34] Bórquez JC, Díaz-Castro F, La Fuente FPD, Espinoza K, Figueroa AM, Martínez-Ruíz I, et al. Mitofusin-2 induced by exercise modifies lipid droplet-mitochondria communication, promoting fatty acid oxidation in male mice with NAFLD. Metabolism: Clinical and Experimental. 2024; 152: 155765. https://doi.org/10.1016/j.metabol.2023.155765
[35] Mitrofanova A, Merscher S, Fornoni A. Kidney lipid dysmetabolism and lipid droplet accumulation in chronic kidney disease. Nature Reviews. Nephrology. 2023; 19: 629–645. https://doi.org/10.1038/s41581-023-00741-w
[36] Wang J, Fang N, Xiong J, Du Y, Cao Y, Ji WK. An ESCRT-dependent step in fatty acid transfer from lipid droplets to mitochondria through VPS13D-TSG101 interactions. Nature Communications. 2021; 12: 1252. https://doi.org/10.1038/s41467-021-21525-5
[37] Miner GE, So CM, Edwards W, Ragusa JV, Wine JT, Wong Gutierrez D, et al. PLIN5 interacts with FATP4 at membrane contact sites to promote lipid droplet-to-mitochondria fatty acid transport. Developmental Cell. 2023; 58: 1250–1265.e6. https://doi.org/10.1016/j.devcel.2023.05.006
[38] Yang M, Luo S, Yang J, Chen W, He L, Liu D, et al. Lipid droplet - mitochondria coupling: A novel lipid metabolism regulatory hub in diabetic nephropathy. Frontiers in Endocrinology. 2022; 13: 1017387. https://doi.org/10.3389/fendo.2022.1017387
[39] Griseti E, Bello AA, Bieth E, Sabbagh B, Iacovoni JS, Bigay J, et al. Molecular mechanisms of perilipin protein function in lipid droplet metabolism. FEBS Letters. 2024; 598: 1170–1198. https://doi.org/10.1002/1873-3468.14792
[40] Jian L, Gao X, Wang C, Sun X, Xu Y, Han R, et al. Perilipin 5 deficiency aggravates cardiac hypertrophy by stimulating lactate production in leptin-deficient mice. Biology Direct. 2023; 18: 54. https://doi.org/10.1186/s13062-023-00411-8
[41] Xu Y, Gao X, Xu S, Jian L, Shi J, Zhao Y, et al. Perilipin 5 enhances glycogen storage and mitigates excessive fatty acid oxidation in skeletal muscle to alleviate mitochondrial impairment. Biochimica Et Biophysica Acta. Molecular Cell Research. 2026; 1873: 120146. https://doi.org/10.1016/j.bbamcr.2026.120146
[42] Aktas G. Exploring the link: Hemogram-derived markers in type 2 diabetes mellitus and its complications. World Journal of Diabetes. 2025; 16: 105233. https://doi.org/10.4239/wjd.v16.i7.105233
[43] Aktas G. Serum C-reactive protein to albumin ratio as a reliable marker of diabetic neuropathy in type 2 diabetes mellitus. Biomolecules & Biomedicine. 2024; 24: 1380–1386. https://doi.org/10.17305/bb.2024.10426
[44] Aktas G. Association between the Prognostic Nutritional Index and Chronic Microvascular Complications in Patients with Type 2 Diabetes Mellitus. Journal of Clinical Medicine. 2023; 12: 5952. https://doi.org/10.3390/jcm12185952